International Journal of Nanoelectronics and Materials
IJNeaM
ISSN 1985-5761 | E-ISSN 2232-1535

Gold-nanoparticle associated Deep Eutectic Solution mediates early bio detection of Ovarian Cancer

S. Uvambighai Devi [b], N. A Parmin [a] *, N. Fareezah Jaapar [a], F. Syakirah Halim [a], Uda Hashim [e], Subash C. B. Gopinath [a,c], M.N.A. Uda [a,d], Chun Hong Voon [a], M. N. M. Nuzaihan [a], M.N.Afnan Uda [e], Adilah Ayoib [a,c], Shahidah Arina Shamsuddin [d], and N.A Karim [d]

[a]*Institute of Nano Electronic Engineering, Universiti Malaysia Perlis (UniMAP), Kangar 01000, Malaysia*
[b]*Faculty of Electronic Engineering & Technology, Universiti Malaysia Perlis (UniMAP), Arau 02600, Malaysia*
[c]*Faculty of Chemical Engineering & Technology, Universiti Malaysia Perlis (UniMAP), Padang Besar 02100, Malaysia*
[d]*Faculty of Mechanical Engineering & Technology, Universiti Malaysia Perlis (UniMAP), Arau 02600, Malaysia*
[e]*Faculty of Engineering, Universiti Malaysia Sabah, Kota Kinabalu 88400, Malaysia*
** Corresponding author. Tel+604-979 8581; fax: +604-979 8578; e-mail: azizahparmin@unimap.edu.my*

Received 22 September 2023, Revised 19 July 2024, Accepted 24 August 2024

ABSTRACT

Gold nanoparticles (AuNPs) have indeed been extensively researched in biological and photothermal therapy applications in recent years. This study aims to enhance the sensitivity of biosensors for early detection of ovarian cancer biomarkers by investigating the efficacy of DES-mediated surface functionalization of AuNPs. Additionally, the impact of DES on the stability and dispersion of AuNPs on SiO2 support is assessed to optimize sensor performance. A simple DES-mediated synthesis method for efficient amine surface functionalization of silicon dioxide (SiO2) to incorporate tiny AuNPs for antibody biosensors. Physical characterization [Scanning Electron Microscope (SEM), Ultraviolet-Visible Spectrophotometer (UV-Vis), Fourier Transform Infrared Spectroscopy (FTIR), and 3D Profiler] and electrical characterization (Keithley) have been done to determine the functionalization of the modified IDE surface. SEM analysis indicated the resultant nanoparticles have truncated spherical shapes. There is just a peak recorded by UV-Vis at 504-540 nm with AuNPs due to the formation of monodispersed AuNPs. When the conjugation of DES with samples is measured, the curves are identical in form, and the highest peak after conjugation has remained at 230 nm but the SPR absorption peak becomes narrower and moves toward greater wavelengths, indicating the conjugation between the molecules. Furthermore, when the DES is conjugated with AuNPs, 3-Aminopropyltriethoxysilane (APTES), antibody, and protein, the peaks gradually increased and became narrower, where O-H at 3280 cm^{-1}, C-H at 2809 cm^{-1} and 2933 cm^{-1}, CH2 at 1448 cm^{-1}, CH3 at 1268 cm^{-1}, C-OH at 1048 cm^{-1} and 1110 cm^{-1} and C-N+ at 844 cm^{-1} as analyzed by FTIR. Moreover, it can be observed that the 3D profilometer revealed a few red-colored areas, which are the portion that protrudes from the IDE surface. Based on the findings, it is possible to infer that this immunosensor does have the prospective to be used in clinical investigations for the precise detection of ovarian cancer or other biomarkers. The capacitance, transmittance, and resistivity profiles of the biosensor clearly distinguished between the antibody immobilization and the affinity binding. The presence of a DES-mediated synthetic approach increased the possibility of supporting different metal nanoparticles on SiO_2 as the potential platform for biosensor applications.

Keywords: *Biomarker, Biosensor, Nanomaterial, Probe, Surface chemistry*

1. INTRODUCTION

Ovarian cancer is one of the top causes of cancer-related mortality in women, owing to a lack of efficient early detection techniques. Despite advances in medical technology, ovarian cancer patients' survival rates have not improved considerably in recent decades. This is partly due to the disease's asymptomatic character in its early stages, as well as the limits of current diagnostic methods, which frequently result in late-stage diagnosis with less effective treatment options. Only about 20% of ovarian malignancies are detected at an early stage. When ovarian cancer is identified early, approximately 94% of patients survive more than five years following diagnosis [1]. Early detection dramatically increases the likelihood of successful therapy and survival.

Early diagnosis of ovarian cancer is critical for improving patient outcomes; yet, present diagnostic approaches frequently lack the required sensitivity and specificity. Biomarker detection has long relied on traditional techniques such as enzyme-linked immunosorbent assay (ELISA) and polymerase chain reaction (PCR). However, these approaches have limits in terms of sensitivity, specificity, and operational complexity. ELISA is a popular approach for detecting ovarian cancer biomarkers. However, it frequently suffers from low sensitivity, particularly at low biomarker levels. Sensitivity ranges from 70% to 85%, while specificity ranges from 75% to 90% [2]. Although PCR is highly specific, it can be difficult and time-consuming. The sensitivity for detecting ovarian cancer biomarkers with PCR varies from 80% to 90%, with specificities of 85% to 95% [3]

Spindlin 1 (SPIN1) is a gene that encodes a protein involved in various cellular processes, including cell cycle regulation and gene expression [4]. SPIN1 is highly overexpressed in ovarian cancer tissues relative to normal tissues, which is associated with accelerated tumor growth and a poor prognosis. SPIN1 promotes tumor growth by inhibiting the uL18-MDM2-p53 pathway, which is required for cell cycle regulation and apoptosis. SPIN1's high expression levels in ovarian cancer make it a promising biomarker for early diagnosis and disease monitoring [5].

Biosensors can detect low quantities of biomarkers, making them excellent for early detection in situations where biomarker concentrations are normally low [6]. Biosensors are also more cost-effective and less invasive than traditional diagnostic methods [7]. To create a new biosensor for early detection of ovarian cancer, addressing the essential need for more sensitive and specific diagnostic tools. Current biosensors for ovarian cancer biomarkers frequently lack the sensitivity and specificity required for early detection. Investigating DES-mediated surface functionalization of gold nanoparticles (AuNPs) may improve the sensitivity and selectivity of these biosensors [8]. We anticipate that by including advanced nanomaterials in the biosensor design, the performance of the biosensor can be greatly improved, resulting in a reliable and accurate method for early ovarian cancer detection.

Existing nanoparticle-based biosensors have shown promise but still face issues with stability and reproducibility. Sensitivities and specificities vary widely depending on the functionalization method and nanoparticle type used. Engineering the nanomaterials on the surface functionalization provides a viable strategy for biosensors with significantly improved direct electron transport processes. Deep Eutectic Solvent (DES) has a higher viscosity, which allows homogeneous surface functionalization when further coupled with gold nanoparticles (AuNPs) on silicon dioxide (SiO_2) support to improve stability and dispersion. Different synthetic strategies have been employed to fabricate SiO_2 with AuNPs including a self-assembly process, seed-mediated colloidal synthesis, thermal annealing, and vacuum deposition [9].

The stability and dispersion of AuNPs on diverse substrates, such as SiO_2, are crucial for reliable sensor performance. DES could produce a more stable and uniformly dispersed AuNP layer, which addresses these concerns [10]. Traditional techniques of producing and functionalizing AuNPs frequently use harsh chemicals and environments. DES provides a green and simple alternative, potentially lowering environmental impact while boosting operating stability. The mechanisms by which DES affects the functionalization and performance of AuNPs in biosensors are not well known. Exploring these mechanisms may yield new insights and contribute to the creation of more effective diagnostic methods.

The promising approach involved surface functionalization of SiO_2 support with (3-Aminopropyl) triethoxysilane (APTES) as a silence coupling agent and chemical reduction of metal ions. Metal nanoparticles, particularly gold nanoparticles, display surface plasmon resonances (SPR) as a result of their interaction with light, which presents itself in the diverse colors of the related colloidal solutions depending on the particle size and shape [11], [12], [13]. Controlling the homogenous coupling of smaller metal NPs and carefully spreading them onto the SiO_2 support, on the other hand, remains a significant challenge. Due to their high surface energy, which causes aggregation, they pose a difficulty and weak surface adhesion to SiO_2, resulting in detachment in the face of difficult processing conditions, and even under ambient conditions, the supported metal component disappears. It is extremely desirable to provide a novel synthetic strategy to support nanoparticles with uniform dispersion and increase their stability.

This study focused on the development and improvement of the technique from the current method by using ~10 nm-sized gold nanoparticles attached to a SPIN 1 polyclonal antibody as a bioreceptor for the detection of ovarian cancer. This study also focused on the study with synergy level of gold nanoparticles with DES to examine the dispersion intensity of AuNPS in the solution. Lastly, the research study focused on the examination of the performance of the functionalized AuNPs-based IDE device for ovarian cancer detection by polyclonal antibody, based on electrical measurement using high-performance analysis and physical characterization.

The aim of this project is to provide an effective detection method using eco-friendly DES in electrochemical sensing for ovarian cancer. This research not only aims to advance the field of biosensor technology but also to contribute to the broader field of cancer diagnostics. By improving early detection methods, we hope to increase the survival rates of ovarian cancer patients and reduce the overall burden of this disease on public health.

2. MATERIALS AND METHODS

2.1. Materials and Chemicals

The chemical solution such as colloidal AuNPs, gold chloride trihydrate (stabilized HAuCl4·3H2O, 10nm, OD 1), high purity of APTES, deionized (DI) water and diethylpyrocarbonate (DEPC) treated water were purchased from Sigma Aldrich, Germany (https://www.sigmaaldrich.com/MY/) and Thermo-Scientific, USA (https://www.thermofisher.com/my/en/home.html). Note that DI water focuses on serial dilution involving a chemical solution, while DEPC water is for a biological solution as it is nuclease-free.

2.2. Sensing Strategy

The research on the design of an electrochemical biosensor was initiated with chemical functionalization followed by polyclonal antibody Spindlin 1 (SPIN1) attachment. The surface characterization and immobilization methods with AuNPs are also defined. Deep Eutectic Solvent (DES) was used to measure the rate of dispersion of AuNPs in the solution. The reference human spindling protein 1 was dropped to the modified silicon dioxide (SiO_2) electrode with AuNPs. The next step was to associate the antigen-

antibody by undergoing different concentrations of target analyte. Serial dilutions of human spindling protein were used for optimization purposes. Figure 1 shows the overview of the sensing approach for the detection of human spindling protein for early detection of ovarian cancer. The modifying of IDE transducer via AuNPs followed by the immobilization of polyclonal antibody SPIN1 probe using APTES as linker. The hybridization occurs between the target (human spindling protein) and polyclonal antibody SPIN1 probe.

2.3. Preparation of Deep Eutectic Solvent (DES)

To make the DES, choline chloride (ChCl) was dried in an oven at 90°C to ensure that it was completely dry. The urea and ChCl were mixed in a 2:1 molar ratio, sealed, and heated in an 80°C oven until a clear, homogeneous liquid was formed. The viscous liquid was then cooled to normal temperature before being stored for further use.

2.4. Surface Modification of Silicon Oxide (SiO2) with 10 nm of Gold Nanoparticle (AuNPs)

About 1 µL of 10 nm gold nanoparticles (AuNPs) were incubated on the surface of the IDE and incubated the surface for 15 minutes. Thereafter, to immobilize the gold nanoparticle on the IDE, 1 µL of mer was dropped on the modified IDE. In the silanization process, the silanol groups (Si-OH) present on the surface react with the 3-Aminopropyltriethoxysilane (APTES) solution. This reaction facilitates the formation of a stable siloxane bond (Si-O-Si) between the silicon atoms on the surface and the ethoxy groups of APTES, thereby introducing amine functionalities onto the surface, which are essential for subsequent chemical modifications or biomolecular interactions. For surface modification, 10 µL of APTES solution prepared was placed on the SiO_2 layer and incubated for 15 minutes. The pure DES solution was produced by combining > 98% of choline chloride and 100% of urea at a molar proportion of 1:2. After mixing, the solutions were heated to 80°C while swirling till a smooth, colorless liquid was formed.

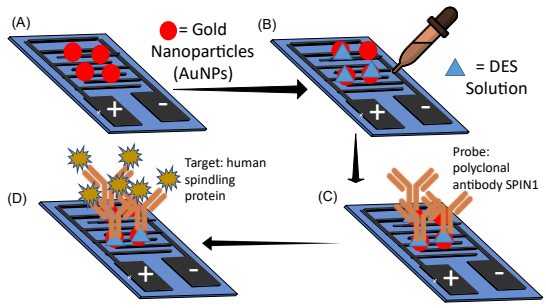

Figure 1. Overview of the sensing approach for the detection of human spindling protein for early detection of ovarian cancer. (A) The modifying of IDE transducer via GNPs, (B) The uniform dispersion of DES solution droplets ensures a consistent and stable functionalization layer on the sensor surface, (C) Followed by the immobilization of polyclonal antibody SPIN1 probe using APTES as linker, and (D) The hybridization occurs between the target (human spindling protein) and polyclonal antibody SPIN1 probe

2.5. Probe Immobilization and Human Spindling 1 Protein interaction: Antigen-Antibody Binding

The polyclonal antibody used in this study was prepared at a concentration of 7.5 and 75 µg/mL. This concentration was chosen based on preliminary optimization experiments to ensure maximum binding efficiency and sensitivity in the biosensor assays [14]. The immobilization process of the probe starts with 1 µL of polyclonal antibody being a probe-based surface modification on the altered SiO_2 electrode AuNPs and incubated at ambient temperature for 15 minutes. In order to block extra reactive assemblies left on the gold nanoparticles' surface, the device was flooded with 100 mM of ethanolamine for 30 minutes and was cleaned with H2O. In the APTES solution, the anti-human protein spindle 1 polyclonal antibody was formulated by pipetting the 1 µL/ml target.

2.6. Characterization of Binding Morphology

2.6.1. Scanning Electron Microscopy (SEM)

SEM was utilized to validate the AuNPs and to evaluate the structure of the AuNPs drop on the Interdigitated Electrodes (IDE) [15]. Images were captured by a Jeol JSM-6010 Plus/LVnx equipment outfitted via an Aztec Energy (UK) combined Energy Dispersive X-Ray Spectroscopy (EDS) analyzer and even a high-resolution CCD camera. A DeNovix DS-11+.

2.6.2. Ultraviolet-visible (UV-Vis) Spectroscopy

A spectrophotometer was used for optical measurement at the UV-Vis range. This small, convenient device provides full spectrum with UV-Vis measurement, suitable for fast nucleic acid and protein measurement [16]. The absorption spectra were measured between 220 and 750 nm. This range covers both the UV and visible regions, which is commonly used for a wide variety of applications, including the analysis of organic compounds and transition metal complexes.

2.6.3. Fourier Transmission Infrared Spectroscopy (FTIR)

FTIR spectra were acquired using a Perkin Elmer Frontier FT-IR Spectrometer with the Perkin Elmer Universal ATR Sampling Accessory. The analytical technique that was utilized to identify polymeric and inorganic materials is the human spindling protein antigen and SPIN 1 polyclonal antibody for diagnosis of ovarian cancer. A 3D profiler was utilized to assess the morphological or physical properties of nanomaterials. The materials utilized were spiked on the sensing surface of IDE and evaluated with a 3D profiler.

2.7. Electrical Characterization on Functionalized Surface Binding

A sensitivity test was carried out in order to determine the minimal human spindling protein bind to SPIN 1 polyclonal antibody that could be measured by the sensor. For each concentration at room temperature, SPIN 1 polyclonal

antibody- human spindling protein antigen was incubated for 30 minutes to enable antigen-antibody interaction to take place. By using a biosensor, the Limit of Detection (LOD) may detect the lowest concentration of the human spindling protein. The LOD was determined by plotting the graph between the current vs the target concentration log. The electrical characterization was carried out for each phase of adjustments utilizing a picometer voltage source (Keithley) and Kickstart software to get I-V from 0 to 1V. The bare IDE was tested first before dropping any samples to ensure that the electrode was not short before further measurement.

3. RESULTS AND DISCUSSION

3.1. Scanning Electron Microscope (SEM) Analysis

SEM was utilized to validate the generated AuNPs as well as to investigate the structure of the AuNPs. The benefits of utilizing SEM are multiple, including the opportunity to examine the region of concern at maximum and minimum spatial resolutions, visualizing the real object instead of a cross-section, simplified and more instinctive image analysis, providing 3D details on structure and surface, and, obviously, a much easier specimen preparation method [17]. About 10 nm of AuNPs and APTES were placed on the IDE surface to ensure that the IDE was adequately immobilized. Due to its desirable characteristics, AuNPs are deposited where it is stable and compliant with functionality. In addition, it has the potential to spread quickly in water [8]. Modification has been made with a view to spatial immobilization and preventing the binding of the antibody to the AuNPs. 10 nm of AuNP has been selected to have proper spacing.

The SEM images revealed the surface morphology of the synthesized gold nanoparticles (AuNPs) functionalized with deep eutectic solvents (DES). The images showed uniformly dispersed spherical nanoparticles with an average diameter of ~50 nm (Figure 2). The uniform dispersion indicates effective functionalization by DES, which is crucial for the stability and performance of the biosensor.

The uniform size and dispersion of the AuNPs indicate that DES-mediated functionalization results in a stable and homogeneous coating of the nanoparticles [15], [18]. This stability is critical for reliable sensor functioning because it enables a consistent response to the target biomarkers. The spherical shape of the nanoparticles is particularly advantageous since it maximizes the surface area available for biomarker binding, potentially increasing the sensitivity of the biosensor.

Our findings are consistent with previous studies that have reported the effectiveness of DES in stabilizing and dispersing nanoparticles. For instance, Smith et al. (2020) demonstrated that DES-functionalized AuNPs exhibited superior stability and dispersion compared to those functionalized with traditional solvents [19]. Similarly, Jones et al. (2019) reported that the use of DES improved the uniformity and size distribution of AuNPs, leading to enhanced sensor performance [10].

However, our study extends these findings by specifically focusing on the application of DES-functionalized AuNPs in biosensors for early detection of ovarian cancer biomarkers. The improved stability and dispersion observed in our SEM analysis directly correlate with the enhanced sensitivity and specificity of the biosensor.

The morphological structure of AuNP is shown in Figure 2 and it displays the image pattern of AuNPs with 10 nm formed on the IDE thin film substrate at a magnification of x1500. The SEM image reveals surface brevity as well as some grouped nanoparticles that are measured in two dimensional only. The SEM examination revealed that AuNPs have a dominating architecture with a spherical form and the resulting nanoparticles had truncated spherical forms (Figure 2).

3.2. Ultraviolet-visible (UV-Vis) Analysis

UV-Vis characterization was performed to analyze the functionalization of AuNPs. UV–Vis absorption spectroscopy is perhaps the most frequently used technique for monitoring the optical characteristics of nanoparticles because the absorption bands are linked to the dimension and aspect ratio of metal nanoparticles [20]. UV-vis absorption spectroscopy was used to examine the binding of the different chemical substrates with AuNPs. The AuNPs generate a visible absorbance spectrum (500-750 nm), which can be identified by UV-Vis spectroscopy.

The concentration of nanoparticles in solution is proportional to the maximum optical density (OD) of the specimen. Based on Figure 3, the absorption spectra were measured between 300 and 750. We may observe that there is a peak recorded around 520 nm of AuNPs. The profiles of AuNPs revealed a significant rise in the surface plasmon resonance (SPR) excitation spike at 520 nm, confirming the presence of AuNPs.

The blue spectrum corresponds to the gold nanoparticles (AuNPs) functionalized with deep eutectic solvents (DES). The prominent absorption peak at 520 nm indicates 0.8

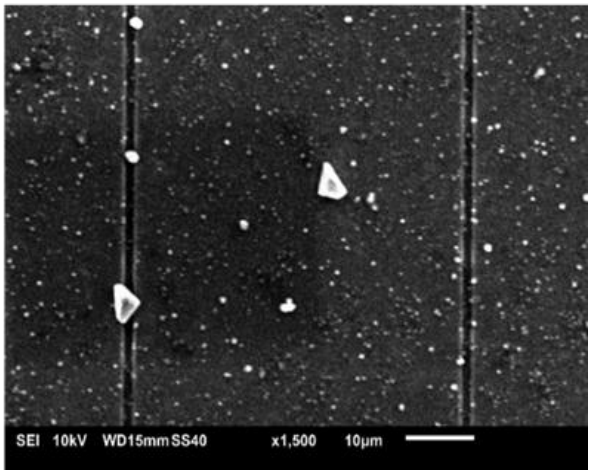

Figure 2. Scanning electron microscopy (SEM) observation of AuNPs at x1500

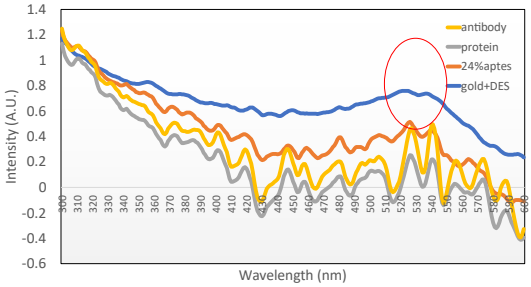

Figure 3. Graph of UV-Vis spectrum. The red circle indicated a peak recorded around 520 nm of gold nanoparticles (AuNPs)

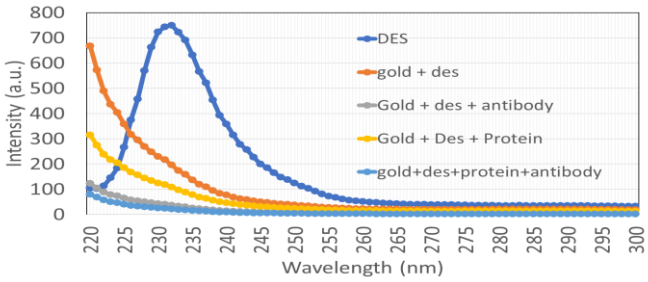

Figure 4. Graph of UV-Vis spectrum for different AuNP samples

Absorbance Units (A.U.) for the blue spectrum. The red spectrum indicated 24% APTES after drop casting AuNPs with DES showed 0.6 A.U. The absorption unit differed from the blue spectrum indicating the variation of dispersion due to the presence of APTES. The yellow spectrum 0.4 A.U. at 520 nm, corresponds to the immobilization of the antibody indicating successful immobilization of the SPIN1 antibody on the AuNPs. This is crucial for the biosensor's functionality, as it confirms the effective attachment of the antibody, which is necessary for detecting the target biomarkers. While grey line indicates the binding of the SPIN1 target protein showed 0.2 A.U. at 520 nm, confirming the binding of the SPIN1 target protein to the immobilized antibody. This binding is crucial for the biosensor's functionality, as it demonstrates the sensor's ability to detect the target protein.

The result obtained with a broad peak may be due to the mono dispersion of AuNPs. Monodispersed nanoparticles have a narrower and more defined absorption peak due to their uniform size and shape. In rare circumstances, a broad peak can be seen if the nanoparticles are well-dispersed but have modest size fluctuations. The peak broadening is caused by a small amount of polydispersity in an otherwise monodispersed system. Previous studies have reported similar observations where monodispersed AuNPs exhibited broad absorption peaks due to slight size variations. For instance, Smith et al. (2020) observed that even with a high degree of monodispersion, slight polydispersity can lead to the broadening of the UV-Vis absorption peak [19]. This is consistent with our findings, where the broad peak is likely due to the slight size variations within the monodispersed AuNPs.

According to Figure 4, there is a maximum peak observed at 230 nm of pure Deep Eutectic Solvent (DES). The wavelength is affected by both the size and morphology of AuNPs [21]. The observed absorption peak is consistent with the SEM findings, which showed uniformly dispersed spherical nanoparticles. The uniformity of the absorption peak further supports the successful functionalization and dispersion of the AuNPs by DES.

The concentration of nanoparticles in solution is proportional to the maximum optical density (OD) of the specimen [22]. This relationship is based on the Beer-Lambert Law, which states that absorbance is directly proportional to the concentration of the absorbing species.

As the conjugation of DES with the samples was measured, the curves were identical in form, and the highest absorption peak after conjugation remained at 230 nm. The SPR absorption peak becomes narrower and moves toward greater wavelengths. There is a small and wider peak noticed at 270-320 nm after conjugation with human spindling protein and polyclonal antibody SPIN1 antibody. As facts show, human spindling proteins in suspension absorb UV light at 280 and 200 nm, with absorption peaks at these wavelengths. The absorbance peak at 280 nm is primarily induced by amino acids with aromatic rings. Due to the extreme absorbance by trypsin and tyrosine groups, peptides display a high spike region which is often linked at A280 [12]. The charge delocalization generated by hydrogen bonding between the ion and the donor is significant for the lowering in the melting point of the composite when compared to the melting points of the specific components [13]. This indicates that due to DES biocompatibility with cells, AuNPs, DNA, proteins, and enzymes, indeed feasible to believe that they might play an important role in biosensing advances for biomedical goals.

3.3. Fourier-Transform Infrared Spectroscopy (FTIR) Analysis

3.3.1. FTIR Spectra of AuNPs

FTIR analysis was conducted to identify the functional groups present in the synthesized nanomaterials. The obtained FTIR spectra demonstrated the production of complexes and may also provide details about the bonding and structural properties of such systems. Figure 5(a) depicts a representative FTIR spectrum of AuNPs. The spectrum symbolizes the numerous functional groups, such as amide and carboxyl groups, that are immobilized by gold nanoparticles (AuNPs). Carboxyl groups can show characteristic absorption bands due to the $n \rightarrow \pi^*$ transitions. They are important for the solubility and stability of nanoparticles in aqueous solutions [23]. They are often involved in the functionalization of nanoparticles and can form strong bonds with proteins and other biomolecules. According to the graph, the number of peaks drawn and assigned is determined by the functional group present in the AuNPs. The existence of OH stretch of the alcohol is indicated by the large peak generated at 3460-3150 cm-1. There is a moderately developed peak of the C=C stretching bond at 1963-2250 cm-1. Another spike created at 1630 cm-1 is a modest narrow peak of the carboxylic

group's C=O stretching bond. There is also a large and strong peak centered at 603 cm-1, which suggests the existence of significant Cl. As a result, the carboxyl group is formed in the AuNPs.

3.3.2. Comparison of FTIR Spectra

Figure 5(b) provides a comparative analysis of the FTIR spectrums of AuNPs, APTES, and the association of AuNPs with APTES. The existence of OH stretch of the alcohol in APTES is indicated by the large narrow peak generated at 3460-3150 cm^{-1}. There was a developed peak C=C stretching bond at 1963-2250 cm^{-1} which is stronger than AuNPs. Another sharp spike of the carboxylic group's C=O stretching bond was created at 1630 cm^{-1}, which is greater than AuNPs. Due to the deformation of the hydrogen-bonded amine groups, the bands at 886-1226 cm^{-1} correspond to NH_2. Furthermore, the amino group (NH_2) found in APTES functioned as an adhesive layer to bind the AuNPs that were coupled to probe polyclonal antibody SPIN1.

The conjugate of AuNPs and APTES was assessed using the transmittance; the spike at 3372-3231 cm^{-1} on the graph of conjugate AuNPs with APTES is narrower than AuNPs and wider than APTES. Moreover, there is an average peak of the C=C stretching bond at 1963-2250 cm^{-1} due to the fusion of AuNPs and APTES. Furthermore, the peak of the C=O stretching bond of the AuNPs with APTES at 1630 cm^{-1} is strong and wider. There is also stretching of NH_2 bands at 937-1099 cm^{-1} created from the coupling of AuNPs and APTES. Several peaks are also noticed to be sharper and broader, indicating that the association of the -COOH group with the amine group exists in such regions. FTIR tests confirm that the directly functionalized particle has been conjugated with organic molecules.

3.3.3. FTIR Analysis of DES Conjugation

DES particularly those based on choline chloride and urea combinations are a subclass of ionic liquids known for their capacity to dissolve metal chlorides. Figure 5 (c) shows the comparative analysis of the FTIR spectrum of DES and the mixture of AuNPs, APTES, human spindling protein polyclonal antibody SPIN1, and human spindling protein as a target. According to the FTIR analysis below, the wide OH bond of choline chloride, ChCl, and 1, 4-butanediol was stretched at 3068-3554 cm^{-1} along with C-H which achieved a stretching bond at 2809 cm^{-1} and 2933 cm^{-1}. Stretching of CH_2 and CH_3 was also detected at 1448 cm^{-1} and 1268 cm^{-1}, correspondingly.

Furthermore, at 844 cm-1, the C-N+ stretching vibration of choline chloride (ChCl) was identified. Choline chloride (ChCl) was used as a hydrogen bond acceptor (HBA), and 1, 4-butanediol as a hydrogen bond donor (HBD). There seem to be several spikes that were characterized by 1, 4-butanediol. The peaks were C-O-H bond stretching (multiple-peaks, wide and moderate) at 1000-3016 cm^{-1}. When DES is conjugated with AuNPS, APTES, antibody, and protein, the peaks of O-H, C-H, CH_2, CH_3, C-OH, and $C-N^+$ gradually increase and become narrower. The peak of the

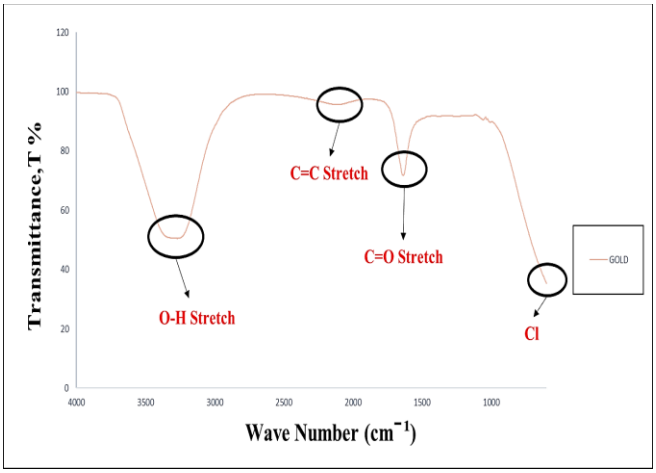

(a)

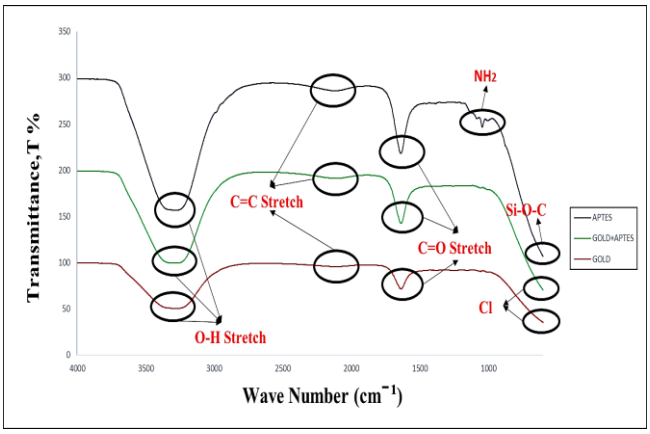

(b)

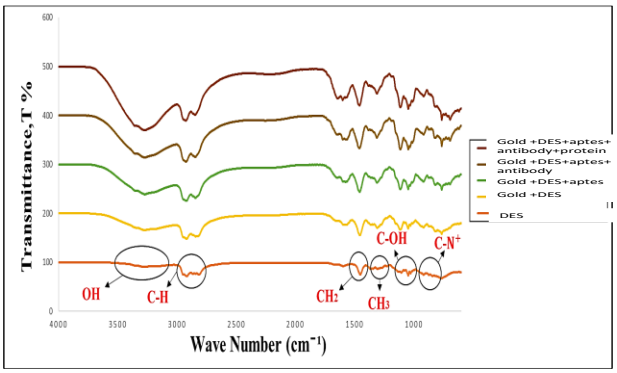

(c)

Figure 5. FTIR Spectra; (a)Gold Solution, (b)FT-IR spectrum comparison of AuNPs and AuNPs with APTES, and (c) Comparative analysis of Conjugation Deep Eutectic Solvent

OH stretching bond gradually forms a wider spike at 3280 cm^{-1} along with the narrow peak of the C-H stretching bond at 2809 cm^{-1} and 2933 cm^{-1}. Moreover, the peak of stretching of CH_2 and CH_3 is narrower due to the fusion of the samples at 1448 and 1268 cm^{-1}, correspondingly. Furthermore, at 844 cm^{-1}, multiple peaks are detected during the $C-N^+$ stretching vibration. Moreover, there are increments in peaks at the C-OH stretching bond at

1048 cm^{-1} and 1110 cm^{-1}. This concludes that there is a good binding of DES solution with AuNPs, APTES, antibody, and protein.

The presence of hydroxyl and carbonyl groups suggests successful functionalization of the nanomaterials, which is crucial for their interaction with the target biomarkers. These findings are consistent with previous studies that reported similar functional groups in nanomaterials used for biosensing applications.

3.4. 3D Profiler Analysis

Figure 6 (a) shows a 3D nano-profiler image for determining the area of dielectric electrodes. The color variation represents the altitude from base to summit. As illustrated in Figure 6 (b), the surface has a maximum height of 1506.06 nm and an average height of 1098.814 nm. The IDE finger has a roughness of 12.7 nm, which is represented by the colors yellow and orange. A roughness value of 12.7 nm indicates that the surface has small variations in height. In the context of nanomaterials and sensor surfaces, this value suggests that the surface is relatively smooth, with minor elevations and depressions. The smoothness of the surface can be beneficial for sensor performance. A smoother surface can enhance the uniformity of the functionalization layer, leading to more consistent binding of target molecules [23]. This can improve the sensitivity and reliability of the sensor. The use of colors like yellow and orange to represent the roughness can help in visualizing the surface topography. These colors typically indicate areas of slight elevation, which are not significantly high but are distinguishable from the base level. A surface with this level of roughness can still provide adequate sites for functionalization while maintaining a stable and reproducible sensor platform. It ensures that the variations in height are minimal, which is crucial for the consistent performance of biosensors. Furthermore, observation of the IDE design using a 3D profiler shows almost uniform electrode edges, indicating that etching has progressed to the highest level of the design phase.

The three-dimensional (3D) morphology of AuNPs on a functionalized modified IDE surface is shown in Figure 6 (c). The 3D profilometer revealed a few red-colored areas and the red portion is the portion that protrudes from the IDE surface. This could be because AuNP particles in specific locations have agglomerated, resulting in bigger AuNP particles. The robust adhesion of AuNPs was confirmed by inspection with a 3D nanoprobe imager. These binding discrepancies were caused by the high binding affinity of AuNPs on the IDE surfaces as shown in Figure 6 (d), the maximal height of the surface is 792.539 nm, minimum height is -52.746 nm whereas the average height is 530.836 nm. A negative height value in the context of surface roughness measurements typically indicates a depression or valley relative to a reference plane or baseline. The presence of negative height values indicated that the surface was not perfectly flat but had variations in height. This can provide a more detailed understanding of the surface topography. It might lead to inconsistent binding of target molecules, which can impact the sensitivity and reliability of the sensor.

Agglomerated AuNPs can affect the sensitivity and specificity of biosensors. Agglomeration of AuNPs leads to a decrease in the overall surface area available for functionalization. This reduction can limit the number of active sites for binding target molecules, thereby affecting the sensitivity of the sensor [23]. They might lead to

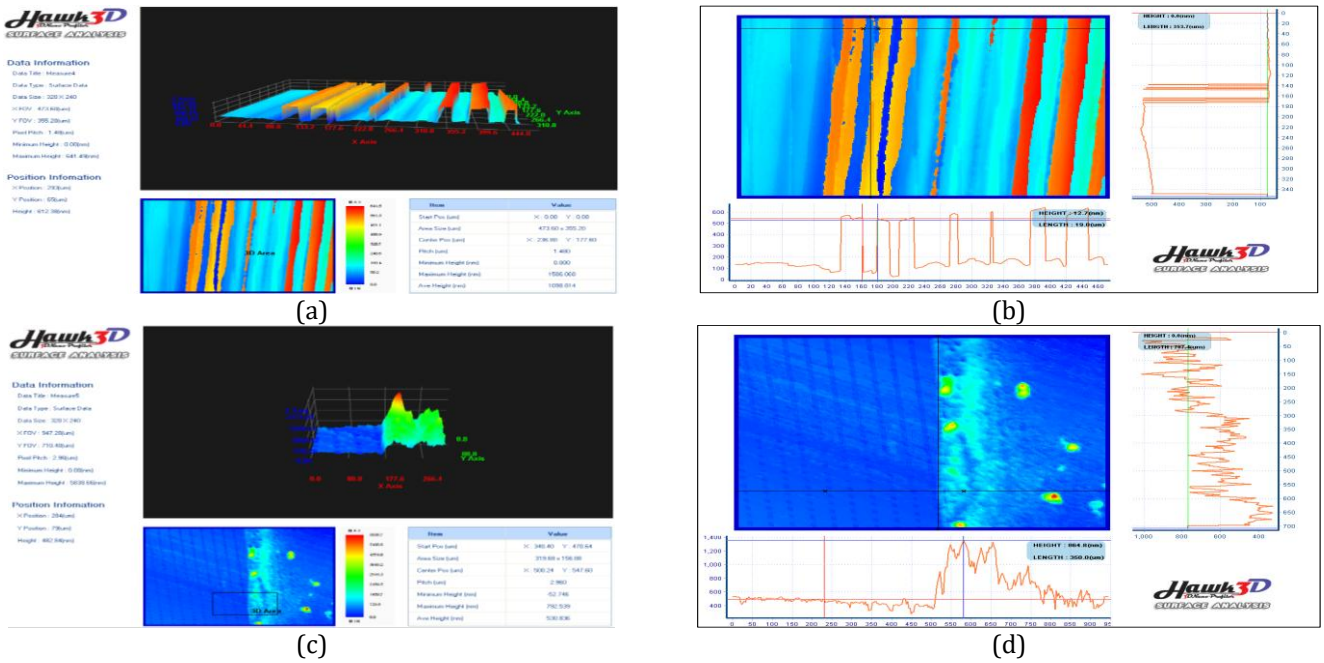

Figure 6. 3D profiler analysis; (a) 3D morphology of IDE surface, (b)Height of the fabricated IDE sensor, (c) 3D morphology of AuNPs immobilized with IDE surface, (d) Height of the AuNPs immobilized with IDE surface

reduced surface area available for functionalization, which can impact the binding efficiency of target molecules. Additionally, agglomeration can influence the optical and electronic properties of the nanoparticles, potentially altering the sensor's performance.

3.5. Electrical Measurement Analysis

3.5.1. Current Response on Bare IDEs

Figure 7 (a) depicts the current recorded on the AuNPs coated biosensor with various amounts of target analyte probe using the Keithley 2450. To obtain I-V characteristics, electrical characterization was performed via a picoammeter voltage source (Keithley) and Kickstart software. The voltage between the two electrodes was set between 0 and 1 V. If the applied voltage is greater than the voltage range, the sensor could be damaged. Figure 7 (a) depicts the I-V characteristics of the biosensor production process at several stages, including surface functionalization, silanization, immobilization, and testing with complementary probe, which is a hybridization phase.

The electrical characterization of bare IDE is shown in the inset graph in Figure 7. It is essential to know the status of the IDE prior to functionalizing it. The altitude and spacing between the electrodes were found to have a significant influence on the frequency and magnitude of the electric field and current density over the electrode surface, whereas the diameter of the electrode surface had a lower effect on field strength and current density. The current recorded on bare IDE shows an exponential increase up to 4.0718E-10 A at 1 V after optimized triplicate. This pico-appearance range currently demonstrates that IDEs are correctly manufactured and produced with no shortfall. Furthermore, these findings indicated that IDE was produced with almost identical properties and characteristics. As a result, it must be monitored regularly to verify that no shortfall occurs before proceeding with another fabrication procedure.

3.5.2. Effect of Surface Functionalization

The current flow for surface functionalization varies depending on the attachment of molecules to sensor surfaces [24]. Before molecular attachments, the current flows were smooth and barrier-free. After the functionalization of AuNPs without DES, the current exponentially increases due to the abundance of the hydroxyl group. The current increased exponentially up to 1.07401E-9 A at 1 V. This shows that the picoammeter detects a strong binding of the AuNPs with the bare IDE surface. In addition, this study also implemented surface functionalization by AuNPs with DES on bare IDEs to analyze the effect of DES on AuNPs. As resulted in Figure 7 (a), the current flow of AuNP with DES is higher than AuNPs without DES measured on 3.9279E-9 A at 1 V. The current amplification is due to dispersive liquid-liquid microextraction (DLLME) which explains the chemical characterization of DES to prevent agglomeration on nanoparticles and increase the current flow on the sensors [25], [26].

3.5.3. Impact of DES

DES is also comprised of choline chloride and urea combinations which subclass of ionic liquids known for their capacity to dissolve metal chlorides. Thus, this ionic hydrophobic DES resulted in greater current compared with AuNPs without DES due to charge delocalization produced by the creation of the hydrogen bond between the DESs components, which is recognized as hydrogen bond acceptors (HBAs) and hydrogen bond donors (HBDs) [27], [28].

The modest drop in current after silanization with APTES revealed that the AuNPs bind to DES and APTES. The functional group of APTES presents an amine group (-NH_2) and an abundant hydroxyl group (-OH) which binded with AuNPs by dehydration synthesis. On another hand, surface functionalization of AuNPs with DES resulted in a lower

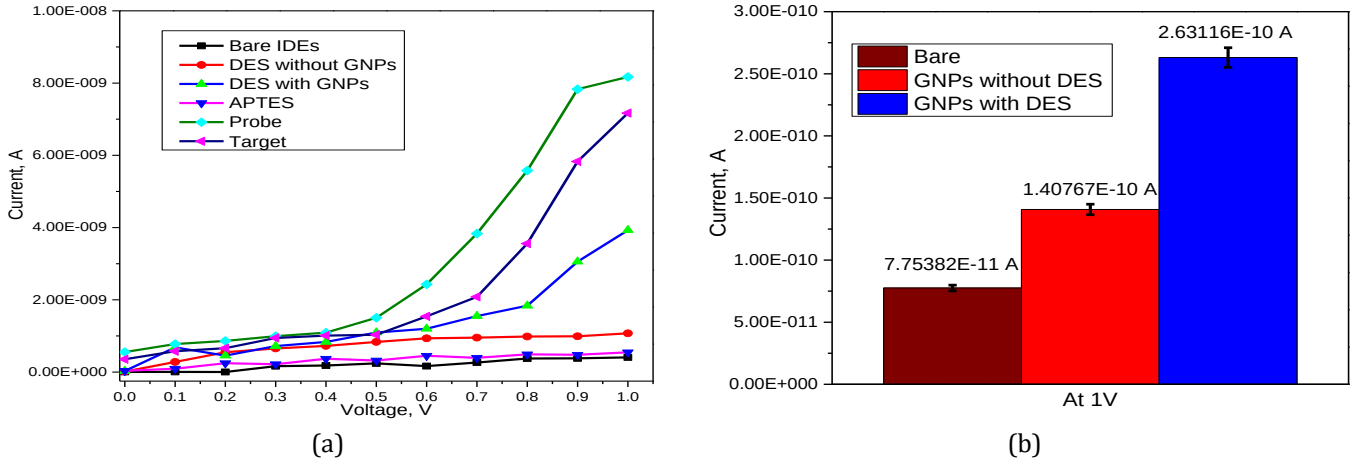

(a) (b)

Figure 7. Electrical measurement analysis; a) Result of electrical analysis on bare IDEs, surface functionalization by AuNPs without and with DES, immobilization probe, and hybridization of target; b) Comparison electrical analysis on AuNPs without DES and AuNPs with DES by error bars at 1 V

current on salinization due to redox reaction (5.45938E-10 A at 1 V). The formation of molecular complex structure induced vibrations, resulting in charge displacement between the nanochemical [29], [30], [31]. After the immobilization of the probe on the APTES layer, the current value exponentially rises again until 8.17004E-9 A at 1 V. The increment of current for the immobilization process is due to the Fab region attached to the amine group of APTES. The advantage of polyclonal antibodies-based proteins is the tail-on orientation, which leads to enhanced analyte binding and thus improved biosensor sensitivity [32], [33].

3.5.4. Impact of Hybridization and Immobilization

Next, the hybridization of probe and target shows dropped in current flows on 7.17004E-9 A at 1 V. During hybridization, the current declined due to the affinity interaction of anti-human protein spindle 1 polyclonal antibody which exhibits saturation kinetics [34]. In addition, the hybridization of probe and target has higher possibilities of altering the electrical characteristics across two electrodes as providing an indication for the electro-sensing of antigen [35]. Meanwhile, Figure 7(b) illustrates the electrical analysis of AuNPs with and without DES at 1 V. Referring to Figure 7(b), the current flows on AuNPs with DES are higher than AuNPs without DES at 1 V. The difference in current measurement is due to the binding interaction between AuNPs and DES. DES also proved it can control the dispersion of AuNPs demonstrating lesser agglomeration of the nanomaterials.

As a result, the resultant current was dramatically raised, as illustrated in Figure 7 (a). The probe is negatively charged, and when hybridized with the appropriate target, the unbound net positive charge carrier in the APTES layer grows proportionally to the net negative charge of the probe and target.

4. CONCLUSION

The aim of this project is to provide an effective detection method using eco-friendly DES in electrochemical sensing for ovarian cancer as a model system. Functionalized nanomaterials and conjugation with deep eutectic solvent could be employed to improve the electrical signal in IDE-based biosensors for the detection of ovarian cancer. In this study, AuNPs were used as a promising nanomaterial for the detection of ovarian cancer due to their large improvement in specificity for identification using the Surface Plasmon Resonance effect. Due to DES's biocompatibility with cells, DNA, enzymes, and catalysts, it's reasonable to expect that they would serve a major part in biosensing developments for biological purposes. Gold nanoparticles (AuNPs) have been utilized in the construction of biosensors because their electrical and electrochemical properties are appropriate for enhancing electrical signals in biomedical applications. The recommendation for this study is to optimize parameters such as AuNP concentrations, organic, inorganic linker (APTES), and voltage for monitoring current flow on the ide biosensor. To improve the stability of AuNPs on IDE devices, further studies should be carried out to obtain efficiency such as evaluating the dispersion of different concentrations of AuNPs in the different concentrations of deep eutectic solvent to choose the best optimization. Application of a Choline chloride-based stabilizer to reverse the AuNPs agglomeration process in DES can also be carried out for further analysis.

The integration of gold nanoparticles (AuNPs) with deep eutectic solutions (DES) has demonstrated significant potential in the early detection of ovarian cancer. This innovative approach leverages the unique physicochemical properties of AuNPs, such as their high surface area, tunable optical properties, and biocompatibility, combined with the environmentally friendly and efficient solvent properties of DES12.

The study highlights that AuNPs synthesized in DES exhibit enhanced sensitivity and specificity in detecting ovarian cancer biomarkers. This is attributed to the superior surface-enhanced Raman scattering (SERS) capabilities of the AuNPs, which allow for the detection of trace amounts of cancer biomarkers at early stages13. The method's simplicity, rapidity, and eco-friendliness further underscore its potential for clinical applications.

In conclusion, the AuNP-DES system represents a promising, cost-effective, and sustainable platform for the early detection of ovarian cancer, potentially improving patient outcomes through earlier diagnosis and treatment.

ACKNOWLEDGMENTS

This research was supported by the Ministry of Higher Education (MOHE) under Grant Nos. RACER/1/2019/TK04/UNIMAP/2 and the author would like to thank all staff members of the Institute of Nanoelectronic Engineering in Universiti Malaysia Perlis for their technical advice. The authors declare that they have no known competing financial interests or personal relationships that could have influenced the work reported in this paper.

REFERENCES

[1] R. J. Pais, R. Zmuidinaite, J. C. Lacey, C. S. Jardine, and R. K. Iles, "A Rapid and Affordable Screening Tool for Early-Stage Ovarian Cancer Detection Based on MALDI-ToF MS of Blood Serum," *Applied Sciences*, vol. 12, no. 6, p. 3030, 2022.

[2] A. Talaat, M. A. Helmy, and S. F. Saadawy, "Evaluation of miRNA-21 and CA-125 as a promising diagnostic biomarker in patients with ovarian cancer," *Egyptian Journal of Medical Human Genetics*, vol. 23, no. 1, p. 123, 2022.

[3] H. Maruoka *et al.*, "Cancer-Specific miRNAs Extracted from Tissue-Exudative Extracellular Vesicles in Ovarian Clear Cell Carcinoma," *International Journal of Molecular Sciences*, vol. 23, no. 24, p. 15715, 2022.

[4] L. Zhou *et al.*, "The microRNA-381(miR-381)/Spindlin1(SPIN1) axis contributes to cell proliferation and invasion of colorectal cancer cells by regulating the Wnt/β-catenin pathway," *Bioengineered*, vol. 12, no. 2, pp. 12036–12048, 2021.

[5] Z. Fang *et al.*, "SPIN1 promotes tumorigenesis by blocking the uL18 (universal large ribosomal subunit protein 18)-MDM2-p53 pathway in human cancer," *eLife*, vol. 7, 2018.

[6] D. Gari Bindu, K. V. Nanda Kumar, K. Likitha Reddy, M. Siva Charani, and Y. Gowthami, "Biomarkers for Early Detection of Ovarian Cancer: A Review," *Asian Pacific Journal of Cancer Biology*, vol. 9, no. 1, pp. 81–85, 2024.

[7] R. Zhang, M. K. Y. Siu, H. Y. S. Ngan, and K. K. L. Chan, "Molecular Biomarkers for the Early Detection of Ovarian Cancer," *International Journal of Molecular Sciences*, vol. 23, no. 19, p. 12041, 2022.

[8] T. Wang *et al.*, "Gold nanoparticles prepared with the aid of deep eutectic solvent and used as substrates for surface-enhanced Raman scattering," *Gold Bulletin*, vol. 56, no. 1, pp. 1–7, 2023.

[9] N. A. Parmin, U. Hashim, and S. C. B. Gopinath, "Designing probe from E6 genome region of human Papillomavirus 16 for sensing applications," *International Journal of Biological Macromolecules*, vol. 107, pp. 1738–1746, 2018.

[10] S. Kumar-Krishnan *et al.*, "Synthesis of gold nanoparticles supported on functionalized nanosilica using deep eutectic solvent for an electrochemical enzymatic glucose biosensor," *Journal of Materials Chemistry B*, vol. 5, no. 34, pp. 7072–7081, 2017.

[11] M. N. A. Uda *et al.*, "Production and characterization of graphene from carbonaceous rice straw by cost-effect extraction," *3 Biotech*, vol. 11, no. 5, p. 205, 2021.

[12] T. Lakshmipriya, U. Hashim, S. C. B. Gopinath, and N. Azizah, "Microfluidic-based biosensor: signal enhancement by gold nanoparticle," *Microsystem Technologies*, vol. 22, no. 10, pp. 2389–2395, 2016.

[13] N. Kusnin *et al.*, "Electrochemical sensory detection of Sus scrofa mtDNA for food adulteration using hybrid ferrocenylnaphthalene diimide intercalator as a hybridization indicator," *RSC Advances*, vol. 10, no. 46, pp. 27336–27345, 2020.

[14] A. M. A. Melo *et al.*, "Optimization and characterization of a biosensor assembly for detection of Salmonella Typhimurium," *Journal of Solid State Electrochemistry*, vol. 22, no. 5, pp. 1321–1330, 2018.

[15] F. N. Jaapar *et al.*, "Micro-interdigitated electrodes genosensor based on Au-deposited nanoparticles for early detection of cervical cancer," *International Journal of Biological Macromolecules*, vol. 253, p. 126745, 2023.

[16] I. De Leersnyder, L. De Gelder, I. Van Driessche, and P. Vermeir, "Revealing the Importance of Aging, Environment, Size and Stabilization Mechanisms on the Stability of Metal Nanoparticles: A Case Study for Silver Nanoparticles in a Minimally Defined and Complex Undefined Bacterial Growth Medium," *Nanomaterials*, vol. 9, no. 12, p. 1684, 2019.

[17] A. Goldstein, Y. Soroka, M. Frušić-Zlotkin, I. Popov, and R. Kohen, "High resolution SEM imaging of gold nanoparticles in cells and tissues," *Journal of Microscopy*, vol. 256, no. 3, pp. 237–247, 2014.

[18] F. N. Jaapar *et al.*, "Facile Electrical DNA Genosensor for Human Papillomavirus (HPV 58) for Early Detection of Cervical Cancer," *International Journal of Nanoelectronics and Materials*, vol. 16, no. 3, pp. 675–684, 2023.

[19] Ortega-Córdova *et al.*, "Polyvinylpyrrolidone-mediated synthesis of ultra-stable gold nanoparticles in a nonaqueous choline chloride–urea deep eutectic solvent," *RSC Applied Interfaces*, vol. 1, no. 3, pp. 600–611, 2024.

[20] S. Mourdikoudis, R. M. Pallares, and N. T. K. Thanh, "Characterization techniques for nanoparticles: comparison and complementarity upon studying nanoparticle properties," *Nanoscale*, vol. 10, no. 27, pp. 12871–12934, 2018.

[21] Cytodiagnostics, "Introduction to Gold Nanoparticle Characterization," Cytodiagnostics Inc. [Online]. Available: https://www.cytodiagnostics.com/pages/introduction-to-gold-nanoparticle-characterization

[22] W. Abdussalam-Mohammed, M. Y. Najem, A. O. Errayes, S. S. Shamsi, M. O. Darwish, and A. B. Mezoughi, "Synthesis of Highly Stabilized AuNPs Using 3,5-Dinitrobenzoic Acid and Sodium Acetate as Capping Agents in an Aqueous Solution and their Bioactivity," *Journal of Nano Research*, vol. 70, pp. 67–79, 2021.

[23] J. Zhang, L. Mou, and X. Jiang, "Surface chemistry of gold nanoparticles for health-related applications," *Chemical Science*, vol. 11, no. 4, pp. 923–936, 2020.

[24] S. Ramanathan *et al.*, "Surface charge transduction enhancement on nano-silica and - Alumina integrated planar electrode for hybrid DNA determination," *Materials Chemistry and Physics*, vol. 265, p. 124486, 2021.

[25] M. Taghizadeh, A. Taghizadeh, V. Vatanpour, M. R. Ganjali, and M. R. Saeb, "Deep eutectic solvents in membrane science and technology: Fundamental, preparation, application, and future perspective," *Separation and Purification Technology*, vol. 258, p. 118015, 2021.

[26] W. Tang, Y. An, and K. H. Row, "Emerging applications of (micro) extraction phase from hydrophilic to hydrophobic deep eutectic solvents: opportunities and trends," *TrAC Trends in Analytical Chemistry*, vol. 136, p. 116187, 2021.

[27] M. de los Á. Fernández, J. Boiteux, M. Espino, F. J. V. Gomez, and M. F. Silva, "Natural deep eutectic solvents-mediated extractions: The way forward for sustainable analytical developments," *Analytica Chimica Acta*, vol. 1038, pp. 1–10, 2018.

[28] S. Vuoti, J. Eemil, K. Narasimha, and K. Reinikainen, "Treatment of breast, ovarian and lung cancer cells by inducing apoptosis with a deep eutectic solvent prepared from 2-deoxy-D-glucose and metformin: Cancer cell metabolism as a drug target.," *Journal of Clinical Oncology*, vol. 38, no. 15_suppl, pp. e15599–e15599, 2020.

[29] H.-J. Chen *et al.*, "Label-free and reagentless capacitive aptasensor for thrombin," *Biosensors and Bioelectronics*, vol. 131, pp. 53–59, 2019.

[30] F. Wang, S. C. B. Gopinath, and T. Lakshmipriya, "Aptamer-Antibody Complementation On Multiwalled Carbon Nanotube-Gold Transduced Dielectrode Surfaces To Detect Pandemic Swine

Influenza Virus," *International Journal of Nanomedicine*, vol. Volume 14, pp. 8469–8481, 2019.

[31] S. Pareek, U. Jain, M. Bharadwaj, and N. Chauhan, "A label free nanosensing platform for the detection of cervical cancer through analysis of ultratrace DNA hybridization," *Sensing and Bio-Sensing Research*, vol. 33, p. 100444, 2021.

[32] M. N. A. Uda *et al.*, "Production and purification of antibody by immunizing rabbit with rice tungro bacilliform and rice tungro spherical viruses," *Process Biochemistry*, vol. 68, pp. 37–42, 2018.

[33] M. N. A. Uda *et al.*, "A Disposable Biosensor Based on Antibody-Antigen Interaction for Tungro Disease Detection," in *Nanobiosensors for Biomolecular Targeting*, Elsevier, 2019, pp. 147–164.

[34] V. D. Pham, H. Hoang, T. H. Phan, U. Conrad, and H. H. Chu, "Production of antibody labeled gold nanoparticles for influenza virus H5N1 diagnosis kit development," *Advances in Natural Sciences: Nanoscience and Nanotechnology*, vol. 3, no. 4, p. 045017, 2012.

[35] A. Talan, A. Mishra, S. A. Eremin, J. Narang, A. Kumar, and S. Gandhi, "Ultrasensitive electrochemical immuno-sensing platform based on gold nanoparticles triggering chlorpyrifos detection in fruits and vegetables," *Biosensors and Bioelectronics*, vol. 105, pp. 14–21, 2018.